

Uncertainty Visualization of 2D Morse Complex Ensembles Using Statistical Summary Maps

Tushar M. Athawale, Dan Maljovec, Lin Yan, Chris R. Johnson, Valerio Pascucci, Bei Wang

Abstract—Morse complexes are gradient-based topological descriptors with close connections to Morse theory. They are widely applicable in scientific visualization as they serve as important abstractions for gaining insights into the topology of scalar fields. Data uncertainty inherent to scalar fields due to randomness in their acquisition and processing, however, limits our understanding of Morse complexes as structural abstractions. We, therefore, explore uncertainty visualization of an ensemble of 2D Morse complexes that arises from scalar fields coupled with data uncertainty. We propose several statistical summary maps as new entities for quantifying structural variations and visualizing positional uncertainties of Morse complexes in ensembles. Specifically, we introduce three types of statistical summary maps – the *probabilistic map*, the *significance map*, and the *survival map* – to characterize the uncertain behaviors of gradient flows. We demonstrate the utility of our proposed approach using wind, flow, and ocean eddy simulation datasets.

Index Terms—Morse complexes, uncertainty visualization, topological data analysis

1 INTRODUCTION

VISUALIZATIONS play an integral role in effective data storytelling and decision-making. Understanding the effects of data uncertainty on visualizations has been recognized as one of the top research challenges [1], [2], [3], [4]. In this paper, we focus on the notion of *aleatoric uncertainty*, which arises due to randomness in data acquisition and processing, and “can not be reduced or removed by model improvements or increases in measurement accuracy” [5]. Uncertainty visualization focuses on improving our ability to reason about the data by communicating their aleatoric uncertainties [5], and it has been shown to be effective in practice [6]. A common practice to mitigate the effects of uncertainty is to combine multiple simulations of a phenomenon (e.g., with varying parameters and/or different instruments) into an ensemble dataset; see [7] for a survey on ensemble visualization.

In this paper, we investigate uncertainty in Morse complexes for an ensemble of 2D scalar fields. Morse complexes and Morse-Smale complexes [8] are topological descriptors based on Morse theory [9], [10] that provide abstract representations of the gradient flow behavior of scalar fields [11]. Morse complexes [8] are the building blocks for Morse-Smale complexes, which have shown great utility in numerous scientific applications, from identifying burning regions in combustion experiments [12] to counting bubbles in mixing fluids [13]. They also appear in partition-based regression [14], [15] and statistical inference [16].

Given a Morse function f defined on a manifold \mathbb{M} , $f : \mathbb{M} \rightarrow \mathbb{R}$, the Morse complex (and Morse-Smale complex) of f decomposes \mathbb{M} into regions (referred to as cells) with uniform gradient behavior (see Sec. 2 for definitions). Morse and Morse-Smale complexes have been extensively studied

under both piecewise-linear (PL) and combinatorial settings (see Sec. 3). However, visualization of these topological descriptors in the face of uncertainty remains challenging.

The uncertainties of Morse complexes capture information about their accuracy, reliability, and variability [1]. In terms of accuracy, Gyulassy et al. [17] have introduced algorithms that improve upon the geometric quality of Morse-Smale complexes. Their algorithms are shown to produce the correct results on average, and the standard deviation approaches zero with increasing mesh resolution. In terms of variability, Thompson et al. [18] have briefly mentioned a Monte Carlo sampling method to quantify variations in the boundaries of Morse cells.

Motivated by limited prior work in encoding uncertainty of topological descriptors [19], [20], we study the uncertainty in Morse complexes for an ensemble of 2D scalar fields. Suppose n ensemble members are given as scalar fields defined on a shared 2D domain, $f_1, \dots, f_n : \mathbb{M} \rightarrow \mathbb{R}$, where $\mathbb{M} \subset \mathbb{R}^2$. We study an ensemble of Morse complexes M_1, \dots, M_n computed from these functions. We assume that each ensemble member f_i is drawn from some distribution that is concentrated around a (potentially unknown) ground truth function f , i.e., $f_i(x) \sim f(x) \pm \epsilon_i(x)$ for any $x \in \mathbb{M}$ (for some $\epsilon_i(x) \geq 0$).

In this work, we propose vector-valued statistical summary maps for encoding and visualizing structural variations of Morse complexes. Specifically, we introduce three types of statistical summary maps to characterize the uncertain behavior of gradient flows and to be utilized in uncertainty visualization for an ensemble: the probabilistic map, the significance map, and the survival map. We give an overview of our computational pipeline in Fig. 1 using a toy example from the Ackley function [21].

In our first type of statistical summary map, the probabilistic map $\mathcal{P} : \mathbb{M} \rightarrow \mathbb{R}^n$, we quantify the uncertainty based on the destination of gradient flows. We assume that by combining persistence simplification [22], [23] with certain labeling strategy (e.g., via k-means clustering, mandatory

• T. M. Athawale, D. Maljovec, L. Yan, C. R. Johnson, V. Pascucci, and B. Wang are with the Scientific Computing & Imaging (SCI) Institute, University of Utah, Salt Lake City, UT, 84112. E-mails: {tushar.athawale, maljovec, linyan, crj, pascucci, beiwang}@sci.utah.edu

Manuscript received April 19, 2005; revised August 26, 2015.

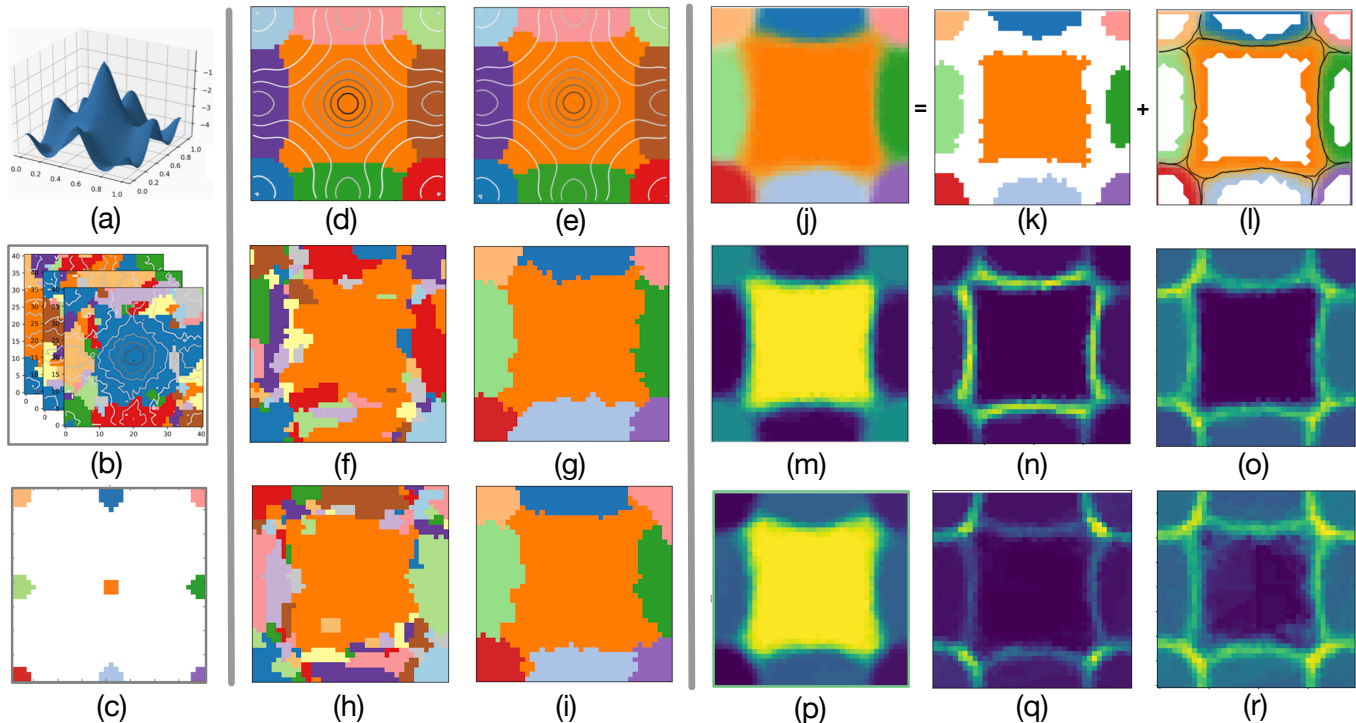


Fig. 1. An overview of our computational pipeline with the Ackley dataset: (a) A 3D visualization of the ground truth Ackley function; (b) an input ensemble of 2D Morse complexes associated with the functions sampled with noise from the ground truth; (c) mandatory local maxima of the ensemble; (d) the Morse complex of the ground truth function; (e) the Morse complex of the mean field; (f-i) two ensemble members before (left) and after (right) persistence simplification; (j-l) a probabilistic map visualized using color blending (j) with certain (k) and uncertain regions (l); (m-o) a significance map visualized with its point-wise mean (m), variance (n), and entropy (o); and (p-r) a survival map visualized with its point-wise mean (p), variance (q), and entropy (r) for the input ensemble. For the yellow-blue diverging colormap, blue means low and yellow means high value.

critical points [24], or Morse mapping [25]), the local maxima of each ensemble member share the same set of labels, denoted as $[l] = \{1, 2, \dots, l\}$. For the Ackley dataset, we have $l = 9$ maxima after persistence simplification (see Figs. 1d-i). Given such a shared labeling, for each point $x \in \mathbb{M}$ in the domain, we compute a probability distribution of its gradient destination across the ensemble. We visualize the probabilistic map using color blending (i.e., weighted mean values) in Figs. 1j-l, where each color represents a distinct label; see Sec. 4 for details.

In our second type of statistical summary map, the significance map $\mathcal{I} : \mathbb{M} \rightarrow \mathbb{R}^n$, we quantify the uncertainty based on the persistence associated with the destination of gradient flows. We assign a *significance measure* to each point $x \in \mathbb{M}$, which is the persistence value of a maximum to which the gradient flow originating at x terminates. We visualize the significance map using point-wise mean, variance, and entropy in Figs. 1m-o, respectively; see Sec. 5 for details.

In our third type of statistical summary map, the survival map $\mathcal{S} : \mathbb{M} \rightarrow \mathbb{R}^n$, we study directional changes of gradient flows as a result of persistence simplification. We assign a *survival measure* for each point $x \in \mathbb{M}$ based on how frequently it changes its gradient destinations during a hierarchical simplification process. We visualize the survival map (Figs. 1p-r) using its point-wise mean, variance, and entropy; see Sec. 6 for details.

Contribution. In summary:

- We quantify the uncertainties in gradient behaviors across a 2D Morse complex ensemble using a proba-

bilistic map \mathcal{P} , a significance map \mathcal{I} , and a survival map \mathcal{S} .

- These vector-valued statistical summary maps capture the uncertainty based upon the variations among gradient destinations (\mathcal{P}), the persistence of these destinations (\mathcal{I}), and the directional changes of gradient flows (\mathcal{S}), respectively.
- These maps employ information obtained during persistence simplification of each ensemble member at a fixed scale (\mathcal{P} and \mathcal{I}) and across all scales (\mathcal{S}), respectively.
- We apply various uncertainty visualization techniques, such as mean-, variance-, and entropy-based visualization, as well as interactive probability queries [26] to our statistical summary maps, to understand the Morse complex structural uncertainty in synthetic and simulation datasets.

2 TECHNICAL BACKGROUND

Our approach has two technical gradients, namely Morse complexes and persistence simplification.

Morse complexes. We focus on the construction of 2D Morse complexes. For simplicity, let $\mathbb{M} \subset \mathbb{R}^2$ be a 2D smooth manifold with a boundary (we further ignore the boundary condition for most of our discussion). Let $f : \mathbb{M} \rightarrow \mathbb{R}$ be a Morse function; ∇f denotes its gradient. A point $x \in \mathbb{M}$ is considered *critical* if $\nabla f(x) = 0$; otherwise it is *regular*. At any regular point x , the gradient is well defined, and integrating it in both ascending and descending directions

traces out an integral line, which is a maximal path whose tangent vectors agree with the gradient [27]. Each integral line begins and ends at critical points. The *descending manifold* surrounding a local maximum is defined as all the points whose integral lines end at the local maximum. The descending manifolds decompose the domain into 2-cells, whereas critical points are the 0-cells, and integral lines connecting the critical points are the 1-cells. As illustrated in Fig. 2a, these cells form a complex called a Morse complex of f , denoted as $M = M_f$ (whenever f is clear from the context). In particular, all the points inside a single 2-cell have their local gradient flows (integral lines) ending at the same local maximum (Fig. 2b).

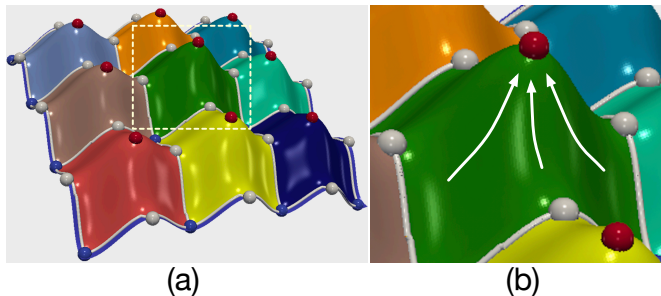


Fig. 2. (a) Descending manifolds forming the Morse complex of f . Colored regions are 2-cells, gray lines are 1-cells. (b) A zoomed-in view of a 2-cell. The white arrows in (b) depict the gradient flows. Red, blue, and gray points are 0-cells that denote local maxima, local minima, and saddles, respectively.

Persistence and persistence simplification. Persistent homology is a tool in topological data analysis for quantifying the significance of topological features. It is widely used for data de-noising through persistence simplification [22]. In visualization, persistence has been used to simplify topological structures, such as Morse and Morse-Smale complexes [8], [28]. For a 2D scalar function, we create a hierarchical Morse complex [22] by simplifying persistence pairs (in this case, maximum-saddle pairs) in the order of increasing persistence values [23]. Persistence assigned to each critical point in the complex intuitively describes the scale at which a critical point disappears through simplification. Persistence pairs can be simplified by successively canceling pairs of critical points connected in the complex with minimal persistence while avoiding certain degenerate situations (see [23] for implementational details).

Fig. 3 illustrates the process of persistence simplification for a 2D Morse complex. A saddle-maximum pair (z, x) with the minimal persistence in Fig. 3a is simplified in Fig. 3c (the respective 2D views are shown in Fig. 3b and Fig. 3d). The process merges the orange cell into the green cell. The gradient flows of all points in the orange cell change their destination from x to y .

3 RELATED WORK

Representations of Morse-Smale complexes. Morse and Morse-Smale complexes are defined for functions on smooth d -manifolds. Moving from the smooth category to the discrete category requires considerable effort to ensure structural integrity and to simulate differentiability [8]. In general, Morse and Morse-Smale complexes can be represented

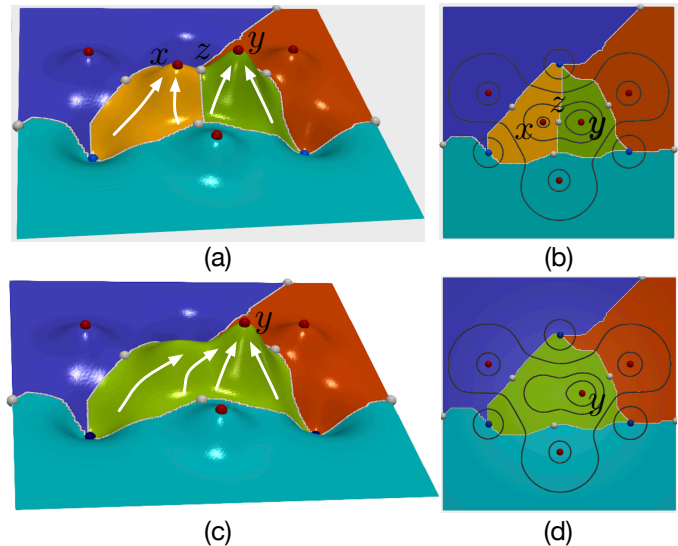


Fig. 3. A 2D Morse complex before (a, b) and after (c, d) persistence simplification. Both 3D (a, c) and 2D views (b, d) of the Morse complexes are shown. A saddle-maximum pair (z, x) in (a) is simplified in (c). White arrows depict the gradient flows.

explicitly or implicitly [23]. The first, an explicit representation, is computed in 2D [8] and 3D [29] for piecewise linear (PL) functions defined on triangulated domains. The second, an implicit representation, originates from Discrete Morse theory [30] where a Morse-Smale complex is implicitly represented by a combinatorial gradient field [23]. We present our results for the explicit representations of Morse complexes, although our methods do not depend upon the choice of the representation. Note that in image analysis, the watershed algorithm [31] is analogous to the computation of Morse complexes in low dimensions.

Uncertainty visualization of critical points and gradient fields. The critical points and induced gradient field of a scalar function characterize the structure of its corresponding Morse complex. A few recent works have focused on data uncertainty and its effects on the critical points and gradient fields. Mihai and Westermann [32] proposed likelihood visualizations of the critical points for an uncertain scalar field, which was extended to Gaussian-distributed uncertain scalar fields by Liebmann and Scheuermann [33]. Huettenberger *et al.* [34] exploited the idea of Pareto optimality for predicting the positions of local extrema for multifield data. Günther *et al.* [24] devised mandatory critical regions as a way to segment the domain of uncertain data, where at least one critical point of an unknown underlying function is guaranteed to exist within a mandatory critical region. Favelier *et al.* [35] developed persistence-based clustering of ensemble members followed by mandatory critical regions for visualizing positional uncertainties of critical points. In this work, we leverage the idea of mandatory critical regions in our probabilistic map (Sec. 4).

Pfaffelmoser *et al.* [36] analyzed the variability in gradient fields induced by uncertain scalar fields, where gradients are computed using the notion of *central differences*. Otto *et al.* [37], [38] proposed Monte Carlo gradient sampling for visualizing variations of pathlines in 2D and 3D uncertain vector fields. Bhatia *et al.* [39] studied *edge maps* for

error analysis of uncertain gradient flows. Nagraj *et al.* [40] proposed a measure to quantify gradient uncertainty for multifield data.

Uncertainty visualization of topological descriptors. A major challenge in visualizing topological descriptors is to encode data uncertainty. Various uncertainty visualization techniques [41], [42], [43] have been proposed to explore structural variations of contour trees for noisy data. Recent work by Yan *et al.* [20] studied structural averages of merge trees in the context of uncertainty visualization. The analysis and visualization of topological variations in the context of uncertain data remains an open research challenge [19].

Several studies have addressed challenges associated with level sets visualization in the face of uncertainty, including contour boxplots [44], probabilistic marching cubes [45], [46], and level set extraction from uncertain data [47], [48], [49]. Multicharts for comparative 3D ensemble visualization [50], dynamic volume lines [51], Gaussian mixture data representations [52], and statistical volume visualization [53] are a few important contributions in volume rendering for visualizing uncertainty.

4 PROBABILISTIC MAP

Using the probabilistic map $\mathcal{P} : \mathbb{M} \rightarrow \mathbb{R}^n$, we quantify the uncertainty based on the destinations of gradient flows. Specifically, for each point $x \in \mathbb{M}$ in the domain, we compute a probability distribution of its gradient destination across the ensemble. Given an ensemble of Morse complexes M_1, \dots, M_n , we combine persistence simplification with a certain labeling strategy to obtain a shared label set for local maxima of the ensemble members. Let $[l] = \{1, 2, \dots, l\}$ denote such a label set. In other words, for each ensemble member M_i , its local maxima have labels that form a subset of $[l]$. Now fix M_i , we trace the gradient flow of each point $x \in \mathbb{M}$ toward its destination, a local maximum $y \in \mathbb{M}$, and assign to x the label of y ; let $\alpha_i : \mathbb{M} \rightarrow [l]$ denote such an assignment. The probabilistic map $\mathcal{P} : \mathbb{M} \rightarrow \mathbb{R}^n$ is defined as a discrete probability distribution of values in $(\alpha_1(x), \alpha_2(x), \dots, \alpha_n(x))$ for each $x \in \mathbb{M}$.

Ackley dataset. We describe our pipeline for the probabilistic map via a synthetic dataset, called the Ackley dataset. Fig. 1a visualizes the Ackley function [21] f as the ground truth. f is made into a Morse function using simulation of simplicity [54]. f contains nine (local) maxima, which produce nine 2-cells in its corresponding Morse complex in Fig. 1d. We generate an ensemble of uncertain scalar fields $\{f_i\}_{i=1}^n$ by mixing f with a small amount of noise sampled from a uniform distribution (i.e., $\epsilon_i(x) \sim U(0, 0.3 \times p_f)$), where p_f is the persistence of the smallest topological feature (a maximum-saddle pair) in f . Two ensemble members $f_i(x) \sim f(x) \pm \epsilon_i(x)$ are shown in Fig. 1f and 1h, respectively. For comparison, we compute the mean field of the ensemble, $\bar{f} = (\sum_i f_i)/n$ and visualize its Morse complex in Fig. 1e. The Morse complex of \bar{f} (Fig. 1e) appears similar to the ground truth (Fig. 1d); however, it does not capture structural variations among the boundaries of 2-cells.

Persistence simplification and labeling. First, we perform a pre-processing step that combines persistence simplification with certain labeling strategy such that the maxima of each

ensemble member share the same set of labels, denoted as $[l] = \{1, 2, \dots, l\}$. There are three labeling strategies, via k-means clustering, mandatory maxima [24], or Morse mapping [25].

For the strategy based on k-means clustering, we use a set of n persistence graphs (Fig. 4a) derived for n ensemble members, each of which shows the number of maxima as a function of persistence [55], to guide the selection of a simplification scale. For a fixed M_i , each maximum has its associate persistence value that indicates at which scale this feature would be simplified, and thus, represents its significance [56]. The shape of the persistence graph, in particular, a plateau, indicates a stable range of scales to separate noise from features [56]. Combining the persistence graphs (Fig. 4a) and spaghetti plots of 1-cells (Fig. 4b) helps us identify a scale for which we observe an agreement in the number maxima across the ensemble. We demonstrate such a process in Fig. 4 where l is determined to be 9 with the aid of persistence graphs and spaghetti plots. We then apply k -means clustering (setting $k = l$) to the maxima across all ensemble members, where each maximum of a simplified \tilde{M}_i is assigned a label in $[l]$.

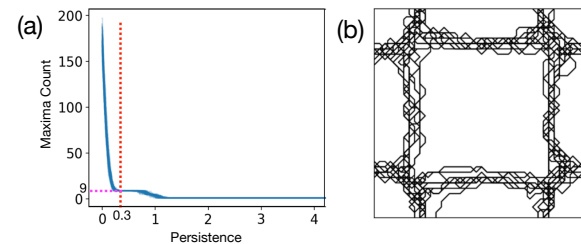


Fig. 4. The persistence simplification process for the Ackley dataset. (a) By overlaying persistence graphs, all ensemble members have the same number (i.e., 9) of maxima (dotted pink line) for a scale at 0.3 within a common stable region (dotted red line). (b) At scale 0.3, overlaid spaghetti plots of 1-cells (i.e., 2-cell boundaries) for the simplified Morse complexes across the ensemble exhibit a significant spatial variation, but the topology of these 1-cells remains consistent.

For the strategy based on mandatory maxima, we apply the technique of Günther *et al.* [24] to an ensemble of uncertain Ackley functions $\{f_i\}_{i=1}^n$, resulting in $l = 9$ mandatory maxima, which are represented by different colors in Fig. 1c. Mandatory maxima are defined to be spatial regions and function ranges where local maxima have to occur across the ensemble [24]. We then apply persistence simplification to each Morse complex M_i until we are left with l maxima. Subsequently, we associate each maxima to its nearest mandatory maxima to obtain its label in $[l]$.

For the strategy based on Morse mapping, we employ a method that has been applied to the tracking of critical points [25]. It builds upon the partition of the domain provided by a Morse complex. For a pair of Morse complexes M_1 and M_2 , we say a maxima $x \in M_1$ is *weakly mapped* to a maxima $y \in M_2$ if x belongs to the 2-cell surrounding y in M_2 . If x is mapped to y and y is mapped to x , then x is *strongly mapped* to y . We choose an ensemble member with a minimum number of maxima as a pivot M_p . For each other member, we assign labels to its maxima by computing both weak and strong mappings against M_p .

Computing the probabilistic map. Now, for each M_i , $\alpha_i : \mathbb{M} \rightarrow [l]$ assigns each $x \in \mathbb{M}$ the label of its

gradient destination (another maxima). The probabilistic map $\mathcal{P} : \mathbb{M} \rightarrow \mathbb{R}^l$ is defined to be a discrete probability distribution of values in $(\alpha_1(x), \dots, \alpha_n(x))$. Let $\mathcal{P}_j(x)$ be the number of times x is assigned a label $j \in [l]$ divided by n . Then $\mathcal{P}(x) = (\mathcal{P}_1(x), \dots, \mathcal{P}_l(x))$. For a point $x \in \mathbb{M}$, if $\mathcal{P}_j(x) = 1$ (implying $\mathcal{P}_k = 0$ for all $k \neq j$) for some j , then x is a *point with certainty*; otherwise, it is a *point with uncertainty*. Points with certainty are those whose gradient flows to the maxima with the same label, whereas points with uncertainty are those whose gradient destinations vary across ensemble members.

Visualizing \mathcal{P} via color blending. Fig. 1j visualizes \mathcal{P} for the Ackley dataset via color blending. Suppose each label is assigned a color, $\{c_1, \dots, c_l\}$, where $c_i \in \mathbb{R}^3$ (a RGB triplet). Point x is then assigned a color as $\sum_i c_i \mathcal{P}_i(x)$. Fig. 1k shows the points with certainty in color. For example, all orange points have their gradients flow to the maxima with the same label. The white regions are points with uncertainty. Points with uncertainty are further visualized with color in Fig. 1l based on their proximity to the points with certainty. For a pair of adjacent regions with different labels i and j (e.g., orange vs. light green), a black contour contains all points $x \in \mathbb{M}$ such that $\mathcal{P}_i(x) = 0.5$ for some label i ; we refer to such black contours as *expected boundaries*.

Visualizing \mathcal{P} via entropy and interactive queries. Furthermore, we compute and visualize point-wise entropy of \mathcal{P} . Given $\mathcal{P} : \mathbb{M} \rightarrow \mathbb{R}^l$, the Shannon entropy [57] at $x \in \mathbb{M}$ is computed as $E(x) = -\sum_{i=1}^l \mathcal{P}_i(x) \log_2 \mathcal{P}_i(x)$. Since uniform probability yields maximum uncertainty and therefore maximum entropy, points with high entropy represent positions whose gradient destinations have higher unpredictability. As illustrated in Fig. 5, points with high entropy ($E \geq 1$) are concentrated within the four corners, because their gradient destinations are (approximately) uniformly distributed across four maxima.

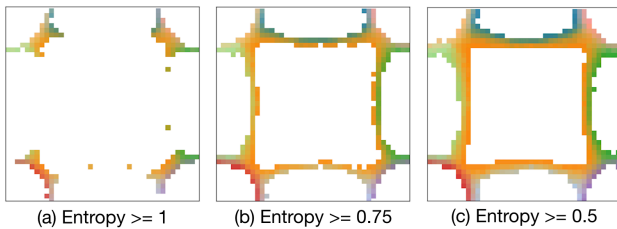


Fig. 5. Visualizing \mathcal{P} with point-wise entropy.

To further understand the points with uncertainty in \mathcal{P} (Fig. 1j), we provide interactive queries based on the framework of Potter *et al.* [26]. Points at selected locations are queried of its corresponding distribution \mathcal{P} (Fig. 6).

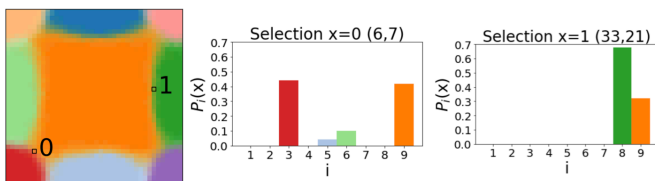


Fig. 6. Interactive queries of \mathcal{P} for the Ackley dataset. Two query locations labeled $x = 0$ and $x = 1$ are selected. $\mathcal{P}_i(x)$ associated with each query location is visualized using a bar chart, where i denotes labels.

5 SIGNIFICANCE MAP

Using the significance map $\mathcal{I} : \mathbb{M} \rightarrow \mathbb{R}^n$, we quantify the uncertainty of a point based on the persistence associated with its gradient destinations at a fixed scale across the ensemble. First, we use *persistence graphs* [55] in combination with spaghetti plots (Fig. 4) to identify the scale of persistence simplification across the ensemble. Second, we apply persistence simplification with the identified simplification scale to each Morse complex M_i . We assign a *significance measure* to each point $x \in \mathbb{M}$ of a simplified ensemble member \tilde{M}_i , which is equal to the persistence value of a local maximum in \tilde{M}_i to which the gradient flow originating at x terminates; let $\beta_i : \mathbb{M} \rightarrow \mathbb{R}$ denote such an assignment. Figs. 7a-b visualize significance assignments across two ensemble members for the Ackley dataset. The significance map $\mathcal{I} : \mathbb{M} \rightarrow \mathbb{R}^n$ is defined to be a vector of significance measures across the ensemble $(\beta_1(x), \beta_2(x), \dots, \beta_n(x))$ for each point $x \in \mathbb{M}$.

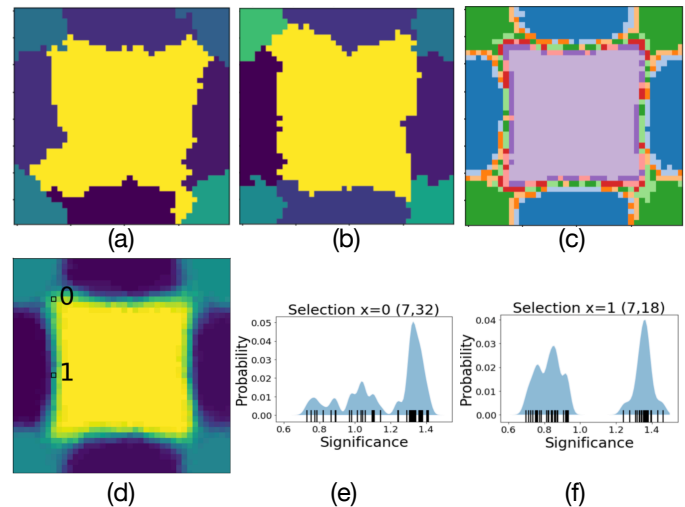


Fig. 7. (a-b) Visualization of significance assignments for two simplified Morse complexes of the Ackley dataset. For the yellow-blue diverging colormap, blue means low and yellow means high value. (c) Quantized visualization of point-wise mean of \mathcal{I} . (d-f) Visualizing the significance map with point-wise mean coupled with interactive queries.

Visualize \mathcal{I} with mean, variance, and entropy. The map \mathcal{I} can be visualized using its point-wise mean, variance, and entropy (Figs. 1m-o). The point-wise mean of \mathcal{I} is defined as $\bar{\beta} := \frac{1}{n} \sum_i \beta_i$. To highlight further the variability of 1-cells, we employ a quantized visualization by dividing the range of \mathcal{I} into a number of intervals and visualize the pre-image of each interval using a miscellaneous colormap (Figs. 7c). The point-wise variance is defined as $\text{Var}(\beta) := \frac{1}{n} \sum_i (\beta_i - \bar{\beta})^2$. The point-wise Shannon entropy is computed by obtaining a probability distributions of the significance values $\beta_1(x), \dots, \beta_n(x)$ using kernel density estimation. For example, via interactive queries, such distributions at the locations with labels $x = 0$ and $x = 1$ are visualized in Figs. 7e-f, respectively.

To capture structural variations in a local neighborhood of a point, we also study variance and entropy computed in a 5×5 patch centered at a given point. This is referred to as the patch-wise variance/entropy. They can be considered as smoothing filters that emphasize and enhance uncertain features in local neighborhoods, see Sec. 7.1 for details.

6 SURVIVAL MAP

Using the survival map $\mathcal{S} : \mathbb{M} \rightarrow \mathbb{R}^n$, we study directional changes of gradient flows as a result of persistence simplification across all scales. For a fixed ensemble member M_i , we first apply a hierarchical persistence simplification of M_i using persistence as a scale parameter. In the case of a 2D Morse complex, we focus on canceling maximum-saddle pairs until only the global maximum remains. We assign a *survival measure* for each point $x \in \mathbb{M}$ based on how frequently it changes its gradient destinations during the simplification process. The less frequently x changes its gradient destinations, the greater is its survival measure, and vice versa. In other words, the survival measure quantifies the *survivability* of consistent flow behaviors. Let $\gamma_i : \mathbb{M} \rightarrow \mathbb{R}$ denote such an assignment. The survival map $\mathcal{S} : \mathbb{M} \rightarrow \mathbb{R}^n$ is defined to be a vector of survival measures across the ensemble, $(\gamma_1(x), \gamma_2(x), \dots, \gamma_n(x))$ for each $x \in \mathbb{M}$.

Algorithmic details. To compute $\gamma : \mathbb{M} \rightarrow \mathbb{R}$ for a particular ensemble member, we use Fig. 3 to illustrate one step of our algorithm with a toy example. Suppose we simplify the maximum-saddle pair (x, z) with the lowest persistence λ . As a result, the gradient flows that terminate at x (Fig. 3a) are redirected to the nearby maxima y (Fig. 3b), effectively merging the orange 2-cell surrounding x into the green 2-cell surrounding y . $\gamma : \mathbb{M} \rightarrow \mathbb{R}$ is increased by λ for all points in the green 2-cell of Fig. 3a, and it is unchanged everywhere else in the domain. In other words, points in the green region (Fig. 3a) have “survived” the simplification without changing their gradient destinations; therefore, they are “rewarded” the amount λ . Therefore, γ captures the *survivability* of local gradient destinations after simplification.

Following the above process, we compute $\gamma_i : \mathbb{M} \rightarrow \mathbb{R}$ for each ensemble member. We initialize γ_i to be zero everywhere. Let $\{\lambda_1, \dots, \lambda_{n_i}\}$ denote the persistence of maximum-saddle pairs to be canceled in an increasing order. We perform n_i steps of persistence simplification. For each step j ($1 \leq j \leq n_i$), γ_i is incremented within a local neighborhood where the gradient flow destinations *survive* (remain unchanged) after simplification. The above process is repeated until the entire Morse complex is simplified into a single 2-cell surrounding the global maximum ($j = n_i$).

Visualize \mathcal{S} with mean, variance, and entropy. Figs. 1p-r visualize \mathcal{S} via its point-wise mean, variance, and entropy, respectively. For instance, the mean is defined as $\mu(x) = \frac{1}{n} \sum_{i=1}^n \gamma_i(x)$. The yellow region in Fig. 1p suggests the existence of a relatively tall peak, and the dark blue regions represent the existence of relatively low peaks across all ensemble members. This behavior is consistent with the ground truth Ackley function depicted in Fig. 1a.

7 RESULTS

We demonstrate the utility of our proposed statistical summary maps for gaining insights into Morse complex uncertainty for simulated and observed scientific datasets.

7.1 Wind Dataset

We first analyze a set of 15 vector fields (velocity) from a wind dataset of the IRI/LDEO Climate Data Library. The

dataset *pressure_level_wind* is obtained using the *NCEP ensemble system*¹ [58] with the *forecast* and *perturbed* parameters. We analyze the dataset with a pressure level at 200 hPa and a forecast hour at 0 on January 01, 2015 over a spatial range of 150°W-49.5°W and 90°N-10°S. The sampling resolution for the grid is 1.5° along each spatial dimension, resulting in a 68x68 grid representing the domain of interest. We obtain an ensemble of 15 Morse complexes computed from the negation of velocity vector magnitudes. That is, we focus on features surrounding the local minima of the velocity magnitude scalar field that correspond to the critical points of vector fields. Fig. 8a shows the mean vector field.

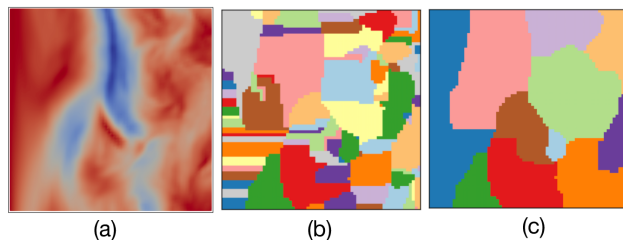


Fig. 8. Wind dataset. (a) Visualization of the negated mean velocity magnitude field (red means low and blue means high velocity magnitude); and its corresponding Morse complexes before (b) and after (c) persistence simplification.

Persistence simplification. Guided by persistence graphs and spaghetti plots, we first apply persistence simplification to obtain a common label set across all ensemble members. From the persistence graphs in Fig. 9a, we identify a common plateau that indicates a stable range of scales to separate features from noise. In particular, at a scale 7 (dotted red line) within the plateau, all members have 11 maxima after simplification (dotted pink line). Spaghetti plots of the simplified Morse complexes with 11 maxima are shown in Fig. 9b. Although there are significant spatial variations of 1-cells, their topology remain sufficiently consistent across the ensemble. Therefore, we analyze the ensemble at the chosen scale where each member contains 11 maxima after simplification.

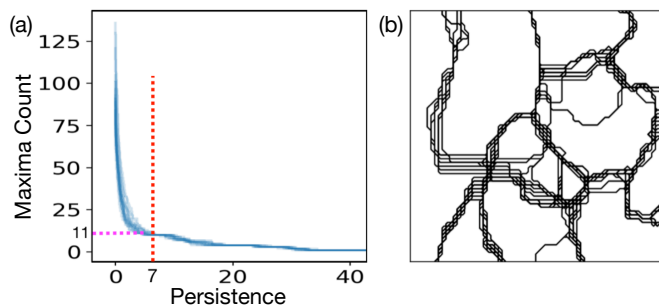


Fig. 9. Wind dataset: persistence simplification. (a) Persistence graphs. (b) Spaghetti plots of the simplified Morse complexes with 11 cells.

For comparison, Fig. 8b visualizes the Morse complex of the mean vector field, which is also simplified to contain 11 maxima in Fig. 8c. Fig. 10 visualizes the Morse complexes for two ensemble members before and after simplification. The spatial variations of 1-cells appear to be substantial, even after simplification. Although persistence simplification of the mean field (Fig. 8c) gives us a high-level view

1. <http://iridl.ldeo.columbia.edu/SOURCES/.ECMWF/.S2S/>

of its gradient behavior, it does not give us insight into positional uncertainties of 1-cells (i.e., 2-cell boundaries).

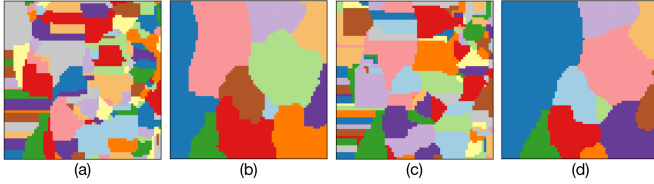


Fig. 10. Wind dataset: Morse complexes of two ensemble members before (a, c) and after (b, d) persistence simplification.

Labeling. Next, we apply k-means clustering to find label correspondences across the simplified ensemble members. Fig. 11a shows a scatter plot of the maxima across simplified ensemble members. Fig. 11b illustrates label correspondences after k-means clustering (where $k = 11$). For comparison, we also experiment with an alternative labeling strategy based on mandatory maxima. Fig. 11c visualizes 11 mandatory maxima computed using the framework of Günther *et al.* [24]. Fig. 11d shows label assignment of each maximum to its nearest mandatory maxima. For the wind dataset, both labeling strategies (k-means vs. mandatory critical points) provide identical results.

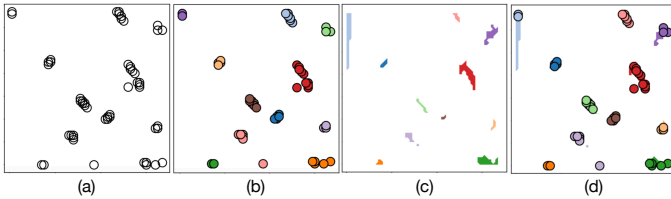


Fig. 11. Labeling with k-means clustering: (a) a scatter plot of maxima across simplified ensemble members; (b) the k-means clustering of maxima with $k = 11$. Labeling with mandatory maxima: (c) mandatory maxima are shown as colored regions; (d) each ensemble maximum is assigned the label of its nearest mandatory maximum.

Probabilistic map. The probabilistic map \mathcal{P} is computed and visualized using color blending in Fig. 12a. In Fig. 12b, \mathcal{P} is visualized based on point-wise entropy (thresholded at ≥ 0.9). Via interactive queries, the gradient flows passing through location $x = 0$ have a high probability of terminating at maxima associated with labels 4 (orange) or 9 (violet); while the gradients passing through $x = 1$ may terminate at maxima with labels 2 (light blue), 6 (red), or 7 (light green).

Significance map. The significance map \mathcal{I} is visualized via its point-wise mean, patch-wise variance, and entropy, as illustrated in Fig. 13. When \mathcal{I} is visualized with its mean in (a) and (b), it captures uncertain segmentation of the domain. In particular, the yellow region in (a) encloses points with high average significance (persistence) and highlights an important feature shared across all members. The regions with higher fluctuations in colors in the quantized visualization (b) represent the positional uncertainty of 1-cells.

The variance-based visualization of \mathcal{I} captures how far a set of significant values is spread out from their mean at a local neighborhood. In particular, the yellow region in Fig. 13d highlights the points with the largest variation. The entropy-based visualization of \mathcal{I} in Fig. 13e highlights neighborhoods that exhibit relatively high random-

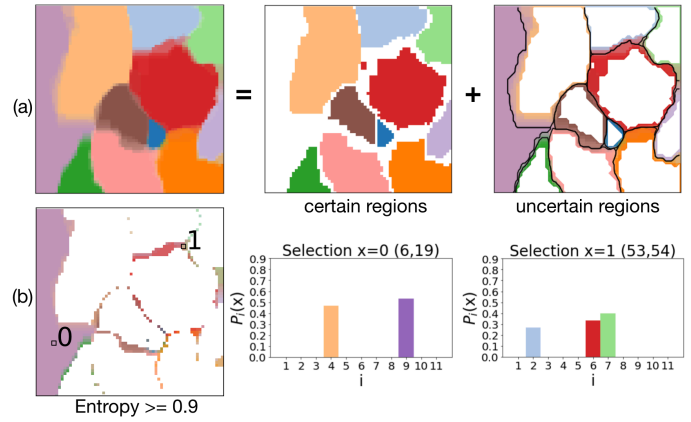


Fig. 12. Wind dataset: (a) \mathcal{P} is visualized using color blending, including points with certainty and points with uncertainty (black contours in the uncertain region denote the expected Morse complex boundaries); (b) \mathcal{P} is visualized based on point-wise entropy thresholded at 0.9.

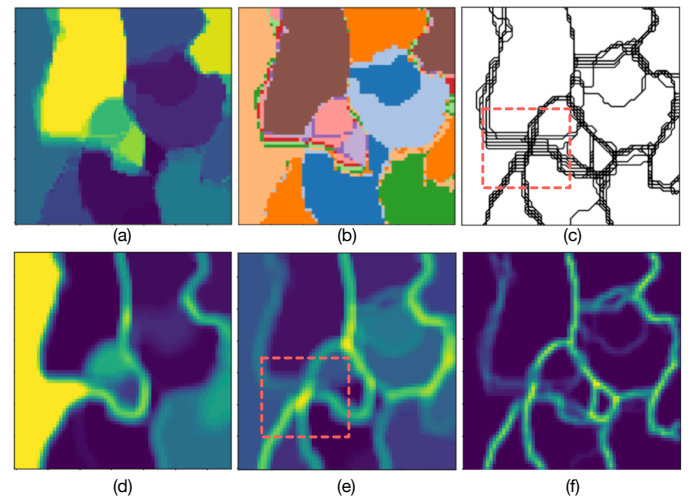


Fig. 13. Wind dataset: (a-b) \mathcal{I} is visualized with its point-wise mean (a), together with its quantized visualization (b); (c) spaghetti plots of 1-cells; (d-e) \mathcal{I} is visualized with its patch-wise variance and entropy, respectively; (f) aggregate segmentation from [18]. For the yellow-blue diverging colormap, blue means low and yellow means high value.

ness in their significance values, thus capturing boundary uncertainty exceptionally well. Points with high entropy, e.g., those enclosed by the red dotted squares in (e), are shown to be consistent with the areas with large spatial variations in the spaghetti plots (c). For comparison, our entropy-based segmentation (e) complements the aggregate segmentation of Thompson *et al.* [18] in (f), which highlights the points that are crossed frequently by the 1-cells across ensembles. It captures the *frequencies* of points serving as 2-cell boundaries, whereas the entropy captures the structural *variabilities* of boundaries in local neighborhoods.

7.2 Navier Stokes Simulation Dataset

We study a time-dependent flow simulation dataset [59]². The dataset originates from a direct numerical Navier Stokes simulation by Camarri *et al.* [59]. It is a 3D flow around a confined square cylinder where the square cylinder has been positioned symmetrically between two parallel walls.

2. <http://tinoweinkauf.net/notes/squarecylinder.html>

Camarri *et al.* used a uniformly resampled version, which was provided by Tino Weinkauff and used by von Funck *et al.* [60] for smoke visualization. We consider an ensemble consisting of velocity vector fields from time steps 60–66 of the 3D simulation. We take a 2D slice perpendicular to the z -axis ($z = 24$) and use velocity magnitude as the underlying scalar fields.

Persistence simplification. First, we apply persistence simplification to obtain a common label set across all ensemble members, guided by persistence graphs and spaghetti plots in Fig. 14. In particular, at the selected simplification scale (dotted red line) in Fig. 14a, 5 out of 7 (70%) members agree on the number of maxima (10) after simplification.

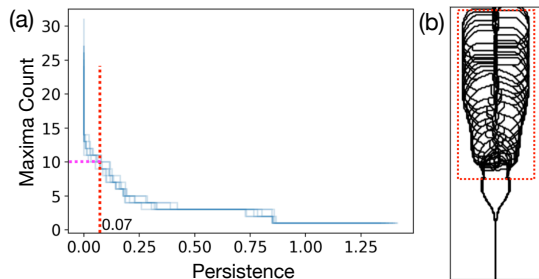


Fig. 14. Navier Stokes simulation dataset: persistence simplification. (a) Persistence graphs. (b) Spaghetti plots of the simplified Morse complexes.

We illustrate three ensemble members at time steps 60, 63, and 66, in Figs. 15a–c, respectively. For each time step, we visualize, from left to right, the underlying scalar field, together with Morse complexes before and after persistence simplification. The mean field (Fig. 15d), on the other hand, misses a significant number of features compared to individual members due to the spatial shift of critical points across the ensemble. Furthermore, the mean field Morse complex does not give any insight into its structural uncertainty.

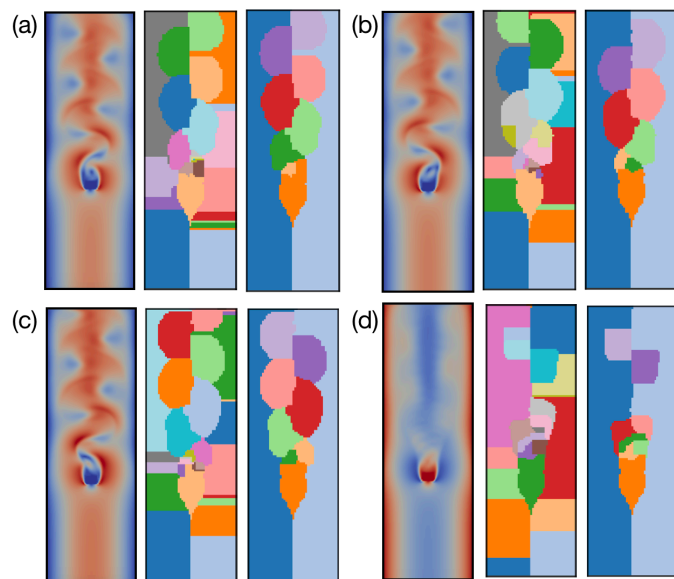


Fig. 15. Navier Stokes simulation dataset. (a–c) Three ensemble members at time steps 60, 63, and 66, respectively. (d) Morse complex of the mean field. Each subfigure visualizes, from left to right, the velocity magnitude field, its corresponding Morse complexes before and after persistence simplification.

However, spaghetti plots of the simplified Morse complexes in Fig. 14b do not display the topological consistency of 1-cells as in Sec. 7.1. For such cases, we demonstrate below how Morse mapping may be an effective strategy for our labeling process.

Labeling. In Fig. 16, we compare the three labeling strategies in finding label correspondences across the simplified ensemble members. Since the mandatory maxima strategy extracts the common denominator of maxima across all ensemble members, its results are sensitive to noise in the data. Specifically, for ensembles with relatively large noise, the number of mandatory maxima tend to be small (3), as illustrated in Fig. 16d. If we simplify each ensemble member to have 3 maxima and assign each maximum the label of its nearest mandatory maximum, we will miss most of the features in the ensemble (Fig. 16e). As illustrated Fig. 16a and Fig. 16(b–c), the Morse mapping and the k -means clustering strategies provide slightly different results. The Morse mapping strategy (Fig. 16a) does not require the simplified ensemble members to have the same number of maxima, and therefore it is more flexible than the k -means clustering.

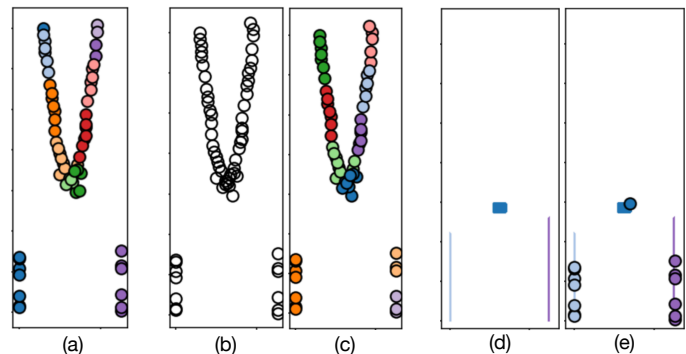


Fig. 16. Navier Stokes simulation dataset. (a) Labeling with Morse mapping. (b–c) Labeling with k -means clustering. (d–e) Labeling with mandatory maxima, which are shown as colored regions in (d); ensemble maxima are labeled with nearest mandatory maxima (e).

Probabilistic map. We further compare and contrast the k -means clustering and Morse mapping labeling strategies for the computation of the probabilistic map \mathcal{P} in Fig. 17. The probabilistic map visualizations using either labeling strategy give insight into the positional uncertainty of the expected 2-cell boundaries that are not observable via the mean field (Fig. 15d). However, as illustrated in Fig. 17b, the expected 2-cell boundaries using Morse mapping appear to be more consistent with respect to the underlying topology of individual ensemble members than those obtained using k -means clustering in Fig. 17a and the mean field in Fig. 15d.

Significance map and survival map. Figs. 18a–c visualize the significance maps \mathcal{I} via point-wise mean, patch-wise variance and entropy, respectively. The region enclosed by the red dotted box within the spaghetti plots in Fig. 14b shows a lack of spatial consistency in the 1-cells across ensemble members. The boundary of such a region is highlighted via the variance in Fig. 18b (white dotted box).

On the other hand, the survival map \mathcal{S} visualized via its mean highlights the yellow feature immediately behind the square cylinder (white dotted box) in Fig. 18d, which has

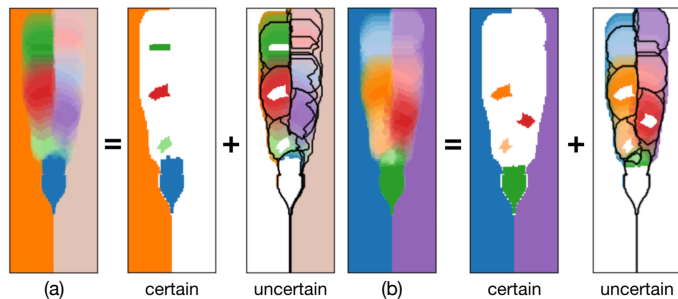


Fig. 17. Navier Stokes simulation dataset: the map \mathcal{P} is computed and visualized based upon k-means clustering (a) and Morse-mapping (b) labeling strategies, respectively. Black contours in the uncertain region denote the expected 2-cell boundaries in both subfigures.

the highest survival measure across all scales. The patch-wise variance and entropy of \mathcal{S} (Figs. 18e-f) both capture high variabilities along its boundaries (white dotted boxes).

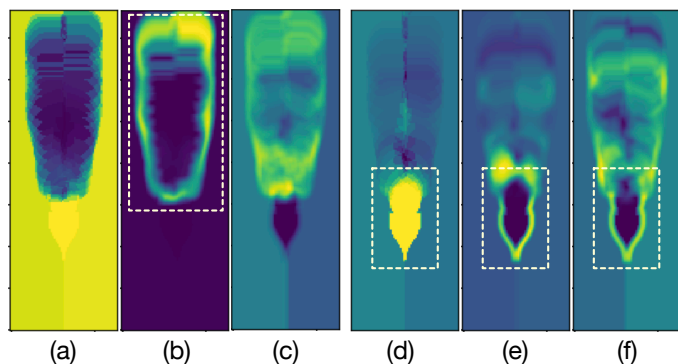


Fig. 18. Navier Stokes simulation dataset: (a-c) \mathcal{I} is visualized with its point-wise mean in (a), patch-wise variance in (b), and patch-wise entropy in (c); (d-f) \mathcal{S} is visualized with its point-wise mean in (d), patch-wise variance in (e), and patch-wise entropy in (f). For the yellow-blue diverging colormap, blue means low and yellow means high value.

7.3 Red Sea Eddy Simulation Dataset

We study the eddy simulation of the Red Sea, which is available via the 2020 IEEE SciVis Contest³. Analyzing the effects of ocean eddies is important in oceanology for gaining insights into the transport of energy and biogeochemical particles [61]. In the Red Sea dataset, each ensemble member is generated based on the MIT ocean general circulation model (MITgcm) and the Data Research Testbed (DART) [62] with varying initial conditions. The data are obtained by sampling from a 3D domain of resolution $500 \times 500 \times 50$, and ensemble members are sampled from 60 time steps to represent a time-varying 3D flow [63]. For our analysis, we use an ensemble of 10 members, in which each member corresponds to a 2D slice perpendicular to the z-axis ($z = 1$) for time step 40. Each ensemble member represents a velocity vector field, and Morse complexes are computed from the negation of velocity magnitudes of each ensemble member to focus on critical points of the vector fields.

Persistence simplification. First, we apply persistence simplification to obtain a common label set across all ensemble members, guided by persistence graphs and spaghetti plots

in Fig. 19. In particular, at the selected simplification scale (dotted red line) in Fig. 19a, 5 of 10 (50%) members agree on the number of maxima (11) after simplification.

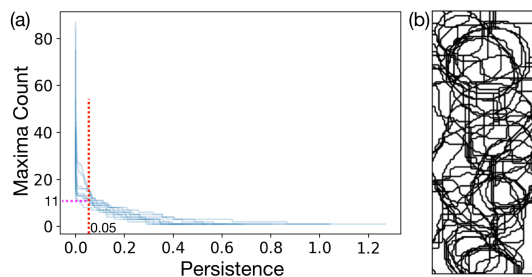


Fig. 19. Red Sea dataset: persistence simplification. (a) Persistence graphs. (b) Spaghetti plots of the simplified Morse complexes.

We illustrate three ensemble members in Figs. 20a-c, respectively. For each ensemble member, its corresponding simplified Morse complex contains 2-cells that highlight vortical features of ocean (white boxes). The mean field Morse complex in Fig. 20d, however, does not give any insight into the structural uncertainty, that is, the variabilities of these features across the ensemble.

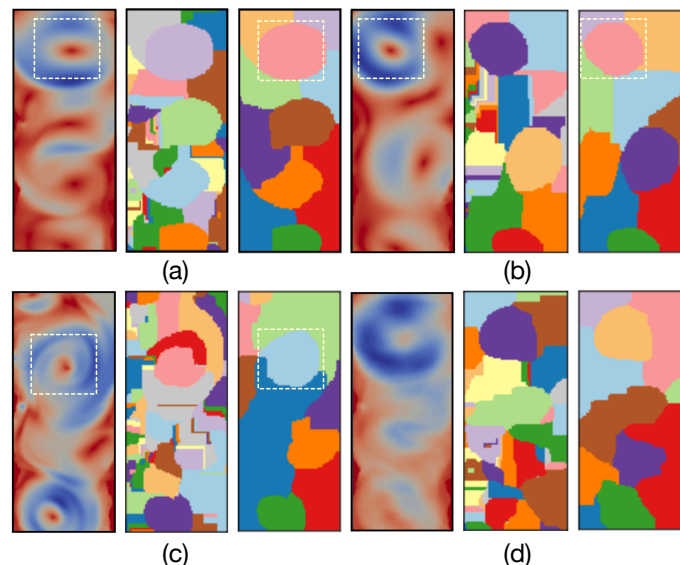


Fig. 20. Red Sea dataset. (a-c) Three ensemble members together with (d) the mean field. Each subfigure visualizes, from left to right, the negated velocity magnitude field (red means low and blue means high velocity magnitude), its corresponding Morse complexes before and after persistence simplification.

On the other hand, spaghetti plots of the simplified Morse complexes in Fig. 19b do not display the topological consistency of 1-cells as in Sec. 7.1. In such cases, we demonstrate below how Morse mapping may be an effective strategy for our labeling process.

Labeling. In Fig. 21, we compare the three labeling strategies. As illustrated in Fig. 21d, the number of mandatory maxima is small (3) since ensemble members have large variations. Simplifying each ensemble member to have 3 maxima will miss most of the features of interest (Fig. 21e). The Morse mapping (Fig. 21a) and the k-means clustering (Fig. 21b-c) strategies, on the other hand, provide reasonable results; the Morse mapping is more flexible without requiring the same number of maxima across the ensemble.

3. <https://kaust-vislab.github.io/SciVis2020/>

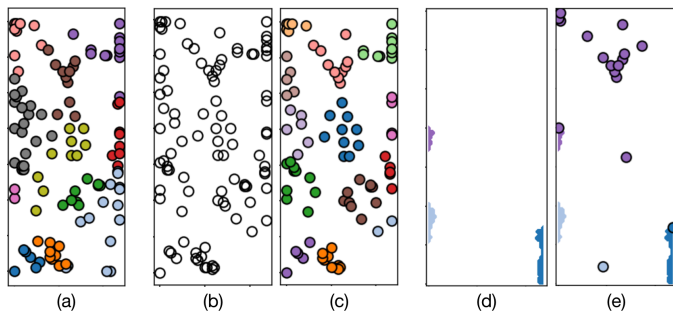


Fig. 21. Red Sea dataset. (a) Labeling with Morse mapping. (b-c) Labeling with k-means clustering. (d) Mandatory maxima are shown as colored regions. (e) Labeling with nearest mandatory maxima.

Probabilistic map. We visualize the probabilistic map using both the k-means clustering and Morse mapping labeling strategies. Both visualizations in Fig. 22 highlight positional uncertainty of 2-cell boundaries invisible to the mean field of Fig. 20d. However, the expected 2-cell boundaries using Morse mapping appear to be more spatially stable than those obtained via k-means clustering.

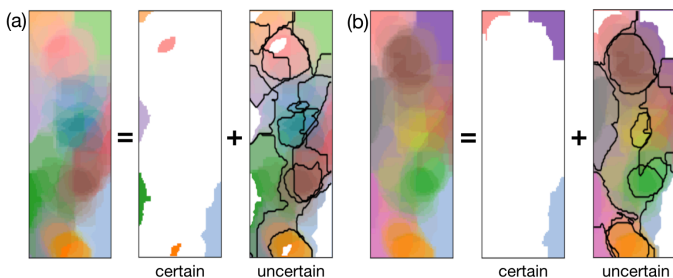


Fig. 22. Red Sea dataset: the map \mathcal{P} is visualized based on (a) k-means clustering and (b) Morse mapping strategies.

Figs. 23a-c visualize our entropy-based exploration of probabilistic map for lower entropy thresholds of 1.5, 1.25, and 1, respectively. Figs. 23d-f carve out regions in the domain, where the ensemble agrees in their gradient destinations for at least 80%, 70%, and 60% members, respectively. Thus, the shared features across the ensemble are discoverable in Figs. 23d-f.

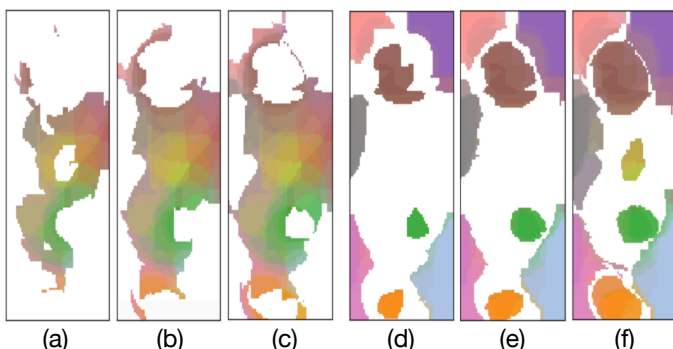


Fig. 23. Red Sea dataset: (a-c) entropy-based exploration of uncertain regions representing entropy greater than or equal to 1.5 in (a), 1.25 in (b), and 1 in (c), respectively; (d-f) visualizations of the regions that agree in their gradient destinations for at least 80% members in (d), 70% members in (e), and 60% members in (f), respectively.

Significance map and survival map. Figs. 24a-c visualize the significance maps \mathcal{I} via point-wise mean, patch-wise

variance and entropy, respectively. The significance map \mathcal{I} in Fig. 24a highlights the presence of a shared feature (white dotted box) with relatively high persistence. The same region (white dotted box) also is of high variance (Fig. 24b) and high entropy (Fig. 24c). Interestingly, the survival map \mathcal{S} appears to be low for this region (white dotted box in Fig. 24d), which requires further investigation.

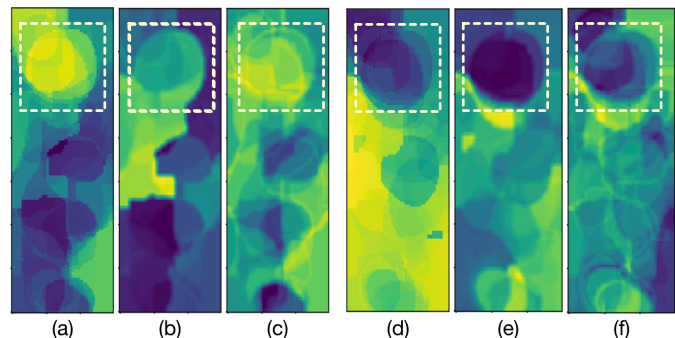


Fig. 24. Red Sea dataset: (a-c) \mathcal{I} is visualized with its point-wise mean in (a), patch-wise variance in (b), and patch-wise entropy in (c); (d-f) \mathcal{S} is visualized with its point-wise mean in (d), patch-wise variance in (e), and patch-wise entropy in (f). For the yellow-blue diverging colormap, blue means low and yellow means high value.

8 CONCLUSION

We propose statistical summary maps as new abstractions for quantifying structural variations among ensembles of Morse complexes that arise from 2D uncertain scalar fields. We introduce three types of statistical summary maps, the probabilistic map \mathcal{P} , the significance map \mathcal{I} , and the survival map \mathcal{S} . We take advantage of persistence simplification, mandatory critical points, or Morse mapping, to derive labeling strategies for ensemble members. We employ techniques such as color blending, entropy-based visualization, interactive queries, and quantized visualizations to understand the structural variability captured by our statistical summary maps.

Regarding labeling strategies, we demonstrate by experiments in Sec. 7.1 and the supplementary material that mandatory maxima capture almost all common features when there is a small amount of noise across the ensemble. However, when the ensemble members become quite noisy, the number of mandatory critical points is significantly smaller than the number of maxima in any ensemble member, rendering the label assignment unreliable (Sec. 7.2 and 7.3). The k-means clustering and the Morse mapping strategies are more general, with the latter being the most flexible when ensemble members are not required to have the same number of maxima.

For future work, we plan to extend our work for Morse complexes beyond 2D. Although Morse complexes may be approximated in higher dimensions, visualizing uncertainties in higher dimensions will require new visual mappings.

ACKNOWLEDGMENTS

This work is supported in part by IIS-1910733, DBI-1661375, and IIS-1513616; the NIH grants P41 GM103545-18 and R24 GM136986; the DOE grant DE-FE0031880; and the Intel Graphics and Visualization Institutes of XELLENCE. We would like to thank Talha Bin Masood for providing us valuable inputs on the Morse mapping strategy and datasets.

REFERENCES

- [1] G. Bonneau, H. Hege, C. R. Johnson, M. Oliveira, K. Potter, and P. Rheingans, "Overview and state-of-the-art of uncertainty visualization," in *Scientific Visualization: Uncertainty, Multifield, Biomedical, and Scalable Visualization*, M. Chen, H. Hagen, C. Hansen, C. R. Johnson, and A. Kauffman, Eds. Springer, 2014, pp. 5–30.
- [2] K. Brodlie, R. O. Allendes, and A. Lopes, "A review of uncertainty in data visualization," *Expanding the Frontiers of Visual Analytics and Visualization*, pp. 81–109, 2012.
- [3] C. R. Johnson and A. R. Sanderson, "A next step: Visualizing errors and uncertainty," *IEEE Computer Graphics and Applications*, vol. 23, no. 5, pp. 6–10, 2003.
- [4] K. Potter, J. Kniss, R. Riesenfeld, and C. R. Johnson, "Visualizing summary statistics and uncertainty," *Computer Graphics Forum*, vol. 29, no. 3, pp. 823–831, 2010.
- [5] K. Potter, P. Rosen, and C. R. Johnson, "From quantification to visualization: A taxonomy of uncertainty visualization approaches," *Uncertainty Quantification in Scientific Computing*, vol. 377, pp. 226–249, 2012.
- [6] J. Hullman, X. Qiao, M. Correll, A. Kale, and M. Kay, "In pursuit of error: A survey of uncertainty visualization evaluation," *IEEE Transactions on Visualization and Computer Graphics*, vol. 25, no. 1, pp. 903–913, 2018.
- [7] J. Wang, S. Hazarika, C. Li, and H.-W. Shen, "Visualization and visual analysis of ensemble data: A survey," *IEEE Transactions on Visualization and Computer Graphics*, vol. 25, no. 9, 2018.
- [8] H. Edelsbrunner, J. Harer, and A. J. Zomorodian, "Hierarchical Morse-Smale complexes for piecewise linear 2-manifolds," *Discrete and Computational Geometry*, vol. 30, pp. 87–107, 2003.
- [9] M. Morse, "Relations between the critical points of a real function of n independent variables," *Transactions of the American Mathematical Society*, vol. 27, no. 3, pp. 345–396, 1925.
- [10] J. Milnor, *Morse Theory*. New Jersey, NY, USA: Princeton University Press, 1963.
- [11] S. Smale, "On gradient dynamical systems," *Annals of Mathematics Second Series*, vol. 74, no. 1, pp. 199–206, 1961.
- [12] P.-T. Bremer, G. Weber, V. Pascucci, M. Day, and J. Bell, "Analyzing and tracking burning structures in lean premixed hydrogen flames," *IEEE Transactions on Visualization and Computer Graphics*, vol. 16, no. 2, pp. 248–260, 2010.
- [13] D. Laney, P.-T. Bremer, A. Mascarenhas, P. Miller, and V. Pascucci, "Understanding the structure of the turbulent mixing layer in hydrodynamic instabilities," *IEEE Transactions on Visualization and Computer Graphics*, vol. 12, no. 5, pp. 1052–1060, 2006.
- [14] S. Gerber, O. Rübél, P.-T. Bremer, V. Pascucci, and R. T. Whitaker, "Morse-Smale regression," *Journal of Computational and Graphical Statistics*, vol. 22, no. 1, pp. 193–214, 2013.
- [15] D. Maljovec, B. Wang, P. Rosen, A. Alfonsi, G. Pastore, C. Rabiti, and V. Pascucci, "Rethinking sensitivity analysis of nuclear simulations with topology," *IEEE Pacific Visualization Symposium*, pp. 64–71, 2016.
- [16] Y.-C. Chen, C. R. Genovese, and L. Wasserman, "Statistical inference using the Morse-Smale complex," *Electronic Journal of Statistics*, vol. 11, no. 1, pp. 1390–1433, 2017.
- [17] A. Gyulassy, P.-T. Bremer, and V. Pascucci, "Computing Morse-Smale complexes with accurate geometry," *IEEE Transactions on Visualization and Computer Graphics*, vol. 18, no. 12, pp. 2014–2022, 2012.
- [18] D. Thompson, J. A. Levine, J. C. Bennett, P.-T. Bremer, A. Gyulassy, and V. Pascucci, "Analysis of large-scale scalar data using hixels," *IEEE Symposium on Large Data Analysis and Visualization*, pp. 23–30, 2011.
- [19] C. Heine, H. Leitte, M. Hlawitschka, F. Iuricich, L. De Floriani, G. Scheuermann, H. Hagen, and C. Garth, "A survey of topology-based methods in visualization," *Computer Graphics Forum*, vol. 35, no. 3, pp. 643–667, 2016.
- [20] L. Yan, Y. Wang, E. Munch, E. Gasparovic, and B. Wang, "A structural average of labeled merge trees for uncertainty visualization," *IEEE Transactions on Visualization and Computer Graphics*, vol. 26, no. 1, pp. 832 – 842, 2020.
- [21] D. H. Ackley, *A connectionist machine for genetic hillclimbing*. Kluwer Academic Publishers Norwell, MA, USA, 1987.
- [22] H. Edelsbrunner, D. Letscher, and A. J. Zomorodian, "Topological persistence and simplification," *Discrete and Computational Geometry*, vol. 28, pp. 511–533, 2002.
- [23] D. Günther, J. Reininghaus, H.-P. Seidel, and T. Weinkauff, "Notes on the simplification of the Morse-Smale complex," in *Topological Methods in Data Analysis and Visualization III*, P.-T. Bremer, I. Hotz, V. Pascucci, and R. Peikert, Eds. Springer International Publishing, 2014, pp. 135–150.
- [24] D. Günther, J. Salmon, and J. Tierny, "Mandatory critical points of 2D uncertain scalar fields," *Computer Graphics Forum*, vol. 33, no. 3, pp. 31–40, 2014.
- [25] J. Reininghaus, J. Kasten, T. Weinkauff, and I. Hotz, "Efficient computation of combinatorial feature flow fields," *IEEE Transactions on Visualization and Computer Graphics*, vol. 18, no. 9, pp. 1563–1573, 2012.
- [26] K. Potter, M. Kirby, D. Xiu, and C. R. Johnson, "Interactive visualization of probability and cumulative density functions," *International Journal for Uncertainty Quantification*, vol. 2, no. 4, pp. 397–412, 2012.
- [27] H. Edelsbrunner, J. Harer, and A. Zomorodian, "Hierarchical Morse complexes for piecewise linear 2-manifolds," in *Proceedings of the 17th Annual Symposium on Computational Geometry*, 2001, pp. 70–79.
- [28] A. Gyulassy and V. Natarajan, "Topology-based simplification for feature extraction from 3D scalar fields," in *IEEE Visualization*, 2005, pp. 535–542.
- [29] H. Edelsbrunner, J. Harer, V. Natarajan, and V. Pascucci, "Morse-Smale complexes for piecewise linear 3-manifolds," *Proceedings of the 19th ACM Symposium on Computational Geometry*, pp. 361–370, 2003.
- [30] R. Forman, "Morse theory for cell complexes," *Advances in Mathematics*, vol. 134, pp. 90–145, 1998.
- [31] S. Beucher and F. Meyer, "The morphological approach to segmentation: The watershed transformation," *Mathematical Morphology in Image Processing*, pp. 433–481, 1993.
- [32] M. Mihai and R. Westermann, "Visualizing the stability of critical points in uncertain scalar fields," *Computers and Graphics*, vol. 41, pp. 13 – 25, 2014.
- [33] T. Liebmann and G. Scheuermann, "Critical points of Gaussian distributed scalar fields on simplicial grids," *Computer Graphics Forum*, vol. 35, no. 3, pp. 361–370, 2016.
- [34] L. Huettenberger, C. Heine, H. Carr, G. Scheuermann, and C. Garth, "Towards multifield scalar topology based on Pareto optimality," *Computer Graphics Forum*, vol. 32, no. 3, pp. 341–350, 2013.
- [35] G. Favelier, N. Faraj, B. Summa, and J. Tierny, "Persistence atlas for critical point variability in ensembles," *IEEE Transactions on Visualization and Computer Graphics*, vol. 25, no. 1, pp. 1152–1162, 2019.
- [36] T. Pfaffelmoser, M. Mihai, and R. Westermann, "Visualizing the variability of gradients in uncertain 2D scalar fields," *IEEE Transactions on Visualization and Computer Graphics*, vol. 19, no. 11, pp. 1948–1961, 2013.
- [37] M. Otto, T. Germer, H.-C. Hege, and H. Theisel, "Uncertain 2D vector field topology," *Computer Graphics Forum*, vol. 29, no. 2, pp. 347–356, 2010.
- [38] M. Otto, T. Germer, and H. Theisel, "Uncertain topology of 3D vector fields," in *IEEE Pacific Visualization Symposium*, 2011, pp. 67–74.
- [39] H. Bhatia, S. Jadhav, P.-T. Bremer, G. Chen, J. Levine, L. Nonato, and V. Pascucci, "Flow visualization with quantified spatial and temporal errors using edge maps," *IEEE Transactions on Visualization and Computer Graphics*, vol. 18, no. 9, pp. 1383–1396, 2012.
- [40] S. Nagaraj, V. Natarajan, and R. S. Nanjundiah, "A gradient-based comparison measure for visual analysis of multifield data reconstruction of gradient in volume rendering," *Eurographics/IEEE Symposium on Visualization*, vol. 30, no. 3, 2011.
- [41] M. Kraus, "Visualization of uncertain contour trees," *Proceedings of the International Conference on Information Visualization Theory and Applications*, pp. 132–139, 2010.
- [42] K. Wu and S. Zhang, "A contour tree based visualization for exploring data with uncertainty," *International Journal for Uncertainty Quantification*, vol. 3, no. 3, pp. 203–223, 2012.
- [43] W. Zhang, P. K. Agarwal, and S. Mukherjee, "Contour trees of uncertain terrains," *Proceedings of the 23rd SIGSPATIAL International Conference on Advances in Geographic Information Systems*, vol. 43, 2015.
- [44] R. Whitaker, M. Mirzargar, and R. Kirby, "Contour boxplots: A method for characterizing uncertainty in feature sets from simu-

- lation ensembles," *IEEE Transactions on Visualization and Computer Graphics*, vol. 19, no. 12, pp. 2713–2722, 2013.
- [45] K. Pöthkow, B. Weber, and H.-C. Hege, "Probabilistic marching cubes," *Computer Graphics Forum*, vol. 30, no. 3, pp. 931–940, 2011.
- [46] K. Pöthkow and H.-C. Hege, "Nonparametric models for uncertainty visualization," *Computer Graphics Forum*, vol. 32, no. 3.2, pp. 131–140, 2013.
- [47] T. Athawale and A. Entezari, "Uncertainty quantification in linear interpolation for isosurface extraction," *IEEE Transactions on Visualization and Computer Graphics*, vol. 19, no. 12, pp. 2723–2732, 2013.
- [48] T. Athawale, E. Sakhæe, and A. Entezari, "Isosurface visualization of data with nonparametric models for uncertainty," *IEEE Transactions on Visualization and Computer Graphics*, vol. 19, no. 12, pp. 2723–2732, 2016.
- [49] T. Athawale and C. R. Johnson, "Probabilistic asymptotic decider for topological ambiguity resolution in level-set extraction for uncertain 2D data," *IEEE Transactions on Visualization and Computer Graphics*, vol. 25, no. 1, pp. 1163–1172, 2019.
- [50] I. Demir, C. Dick, and R. Westermann, "Multi-charts for comparative 3D ensemble visualization," *IEEE Transactions on Visualization and Computer Graphics*, vol. 20, no. 12, pp. 2694–2703, 2014.
- [51] J. Weissenböck, B. Frohler, E. Groller, J. Kastner, and C. Heinzl, "Dynamic volume lines: Visual comparison of 3D volumes through space-filling curves," *IEEE Transactions on Visualization and Computer Graphics*, vol. 25, no. 1, pp. 1040–1049, 2019.
- [52] S. Liu, J. Levine, P.-T. Bremer, and V. Pascucci, "Gaussian mixture model based volume visualization," in *Proceedings of the IEEE Large-Scale Data Analysis and Visualization Symposium*, 2012, pp. 73–77.
- [53] E. Sakhæe and A. Entezari, "A statistical direct volume rendering framework for visualization of uncertain data," *IEEE Transactions on Visualization and Computer Graphics*, vol. 23, no. 12, pp. 2509–2520, 2017.
- [54] H. Edelsbrunner and E. P. Mücke, "Simulation of simplicity: A technique to cope with degenerate cases in geometric algorithms," *ACM Transactions on Graphics*, vol. 9, pp. 66–104, 1990.
- [55] S. Gerber, P.-T. Bremer, V. Pascucci, and R. Whitaker, "Visual exploration of high dimensional scalar functions," *IEEE Transactions on Visualization and Computer Graphics*, vol. 16, pp. 1271–1280, 2010.
- [56] P.-T. Bremer, D. Maljovec, A. Saha, B. Wang, J. Gaffney, B. K. Spears, and V. Pascucci, "ND2AV: N-dimensional data analysis and visualization – analysis for the national ignition campaign," *Computing and Visualization in Science*, vol. 17, no. 1, pp. 1–18, 2015.
- [57] C. E. Shannon, "A mathematical theory of communication," *Bell System Technical Journal*, vol. 27, no. 3, pp. 379–423, 1948.
- [58] F. Vitart et al., "The subseasonal to seasonal (S2S) prediction project database," *Bulletin of the American Meteorological Society*, vol. 98, pp. 163–173, 2017.
- [59] S. Camarri, M.-V. Salvetti, M. Buffoni, and A. Iollo, "Simulation of the three-dimensional flow around a square cylinder between parallel walls at moderate Reynolds numbers," *XVII Congresso di Meccanica Teorica ed Applicata*, 2005.
- [60] W. von Funck, T. Weinkauff, H. Theisel, and H.-P. Seidel, "Smoke surfaces: An interactive flow visualization technique inspired by real-world flow experiments," *IEEE Transactions on Visualization and Computer Graphics*, vol. 14, no. 6, pp. 1396–1403, 2008.
- [61] P. Zhan, G. Krokos, D. Guo, and I. Hoteit, "Three-dimensional signature of the Red Sea eddies and eddy-induced transport," *Geophysical Research Letters*, vol. 46, no. 4, pp. 2167–2177, 2019.
- [62] I. Hoteit, T. Hoar, G. Gopalakrishnan, Nancy Collins, J. Anderson, B. Cornuelle, A. Köhld, and P. Heimbach, "A MITgcm/DART ocean analysis and prediction system with application to the Gulf of Mexico," *Dynamics of Atmospheres and Oceans*, vol. 63, pp. 1–23, 2013.
- [63] S. Sivareddy, H. Toye, P. Zhan, S. Langodan, G. Krokos, O. Knio, and I. Hoteit, "Impact of atmospheric and model physics perturbations on a high-resolution ensemble data assimilation system of the Red Sea," *Journal of Geophysical Research: Oceans*, 2020.



Tushar Athawale is a postdoctoral fellow at the University of Utah's Scientific Computing & Imaging (SCI) Institute. He received Ph.D. in Computer Science from the University of Florida in May, 2015. He was a full-time employee at MathWorks, Inc., before joining the SCI institute. His primary research interests are in uncertainty visualization and statistical analysis for scientific data. Tushar completed his B.S. in Computer Engineering from the University of Pune, India.



Dan Maljovec got his Ph.D. from the School of Computing at the University of Utah where he focused on the application of topological models to high dimensional data. He received his B.S. in Computer Science from Gannon University in 2009. He was a research assistant at the SCI Institute since 2012. He is now a full-time employee at Recursion Pharmaceuticals at Salt Lake City.



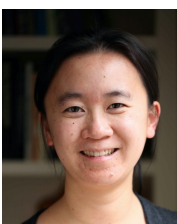
Lin Yan is a Ph.D. student from the School of Computing and the Scientific Computing & Imaging (SCI) Institute at the University of Utah. She received her B.S. and M.S. from Shanghai Jiao Tong University, China (M.S. in Control Science and Engineering, and B.S. in Automation). Her research interests are topological data analysis and scientific data visualization of high-dimensional point clouds, scalar fields, vector fields, and tensor fields.



Chris R. Johnson is a Distinguished Professor of Computer Science and founding director of the Scientific Computing & Imaging (SCI) Institute at the University of Utah. With Charles Hansen, he co-edited the Visualization Handbook. He is a Fellow of AIMBE (2004), AAAS (2005), SIAM (2009), and IEEE (2014) and has received multiple research awards, including the NSF Presidential Faculty Fellow award from President Clinton, the Governor's Medal for Science and Technology, the Utah Cyber Pioneer Award, the IEEE Visualization Career Award, the IEEE IPDPS Charles Babbage Award, the IEEE Sidney Fernbach Award, and the University of Utah's most prestigious faculty award, the Rosenblatt Prize.



Valerio Pascucci is the John R. Parks Inaugural Endowed Chair and the founding Director of the Center for Extreme Data Management Analysis and Visualization (CEDMAV) of the University of Utah. Valerio is also a Faculty of the SCI Institute, a Professor of the School of Computing, University of Utah. His research interests include big data management and analytics, progressive multi-resolution techniques in scientific visualization, discrete topology, geometric compression, computer graphics, computational geometry, geometric programming, and solid modeling.



Bei Wang is an assistant professor at the School of Computing and a faculty member at the Scientific Computing and Imaging (SCI) Institute, University of Utah. She received her Ph.D. in Computer Science from Duke University. She is interested in the analysis and visualization of large and complex data. Her research interests include topological data analysis, data visualization, computational topology, computational geometry, machine learning and data mining.